Article

Research on the Decoupling of the Parallel Vehicle Tilting and Steering Mechanism

Ruolin Gao [1], Haitao Li [1,*], Wenjun Wei [1,2] and Ya Wang [2]

1   College of Engineering, China Agricultural University, Beijing 100083, China; grlbest@cau.edu.cn (R.G.); mech01@cau.edu.cn (W.W.)
2   Beijing Zuoqi Technology Co., Ltd., Beijing 100083, China; wangyaqc@sohu.com
*   Correspondence: h.li@cau.edu.cn; Tel.: +86-132-4096-7299

Featured Application: The authors were encouraged to provide an active tilting vehicle suspension design method. The study method is suitable for decoupling various spatial parallel mechanisms.

Abstract: Active tilting vehicles tilt to the inside of the corner when the vehicle is steering. The tilting motion improves the steering and roll stability of the vehicle. The steering mechanism and the tilting mechanism of the vehicle are connected in parallel. The transmission of the steering mechanism is influenced by the movements of the tilting mechanism. In order to solve this problem, a parallel mechanism is proposed in this paper. It consists of a spatial steering mechanism and a tilting mechanism in parallel. A mathematical model of the parallel mechanism with the wheel alignment parameters has been established. The model calculates the decoupling conditions of the parallel mechanism. In this study, a decoupling method for the parallel mechanism is proposed. A prototype of the parallel mechanism was designed according to the proposed method. The prototype was found to reduce the influence of vehicle tilting on the outer and inner wheel steering angles by up to 0.64% and 0.78%, respectively. The steering geometry correction rate of the prototype is between 1.198 and 0.961. The correctness of the model was verified by experimentation on the prototype. The proposed method can effectively decouple the tilting motion and steering motion of the vehicle and make the wheels on both sides satisfy the Ackerman steering condition.

Keywords: parallel mechanism; spatial steering mechanism; tilting mechanism; mechanism decoupling; active tilting vehicle; wheel alignment parameters

1. Introduction

The burden of urban road traffic is steadily growing as car safety performance improves. This problem and the progress of vehicle technology have created new interest in narrow-body vehicles for individual mobility [1]. Narrow-body vehicles are often only provided for use by a single driver or shared by a driver and a passenger [2]. This is the reason why narrow-body vehicles can save public road resources. Compared with two-wheeled motorcycles, this type of vehicle has the ability to shield from wind and rain, which improves the driver's comfort level. Compared with ordinary four-wheeled cars, this type of vehicle has a narrower body and is more maneuverable on urban roads. This type of vehicle is mainly used in urban commuting as a replacement for low-speed cars [3]. The relatively high center of gravity makes the narrow-body vehicle prone to rollover. Traditional narrow-body vehicles prevent rollover by installing stabilizer bars. This method reduces the ride comfort of the vehicle [4]. Active tilting vehicles (ATV) can solve the contradiction between preventing rollover and improving ride comfort [5].

ATV actively tilt to the inside of the curve by a certain angle. The gravitational moment that is generated by the tilting motion is used to counteract the centrifugal moment [6,7]. The tilt motion can avoid vehicle turnover [8,9]. The steering mechanism and tilting

mechanism of the vehicle are connected in parallel. Some design methods for a tilting and steering mechanism have been proposed [10,11].

When the tilting mechanism drives the vehicle tilting to the left, all of the wheels of the vehicle on the left side move up and the wheels on the right side move down in relation to the position of the vehicle [11]. When the vehicle tilts to the right, the movement of the wheels is reversed. The swingarm connecting the kingpin in the tilting mechanism is longer than that which is found in typical wishbone suspension. It has a broader range of movement that allows it to tilt the vehicle at a greater angle [10]. The steering mechanism also has to direct the wheels on the left and right sides by use of the swingarm and steering rod. As such, the movements of the tilting mechanism will influence the transmission of the steering mechanism.

One option to solve this problem is to split the tilting mechanism and the steering mechanism into two independent mechanisms [1]. W. A. Grzegoek and S. Ishino designed tilting mechanisms that steer by the use of an independent wheel [1,12]. Y. H. Cho et al. connected two mechanisms in series. This tandem mechanism used separate actuators to control the tilting motion and steering motion of the vehicle [13]. These methods add a lot of costs.

Connecting the steering mechanism and the tilting mechanism in parallel is a low-cost method that can realize two-wheel steering [11]. Q. Sun et al. and X. L. Bian et al. used planar four-bar linkage as the steering mechanism. The mechanism parameters which realize the Ackerman steering condition (ASC) were obtained [14,15]. J. Zhao et al. designed a vehicle steering mechanism with incomplete non-circular gears [16]. The mechanism can reduce the deviation between the actual steering angle of the wheel and the steering angle that satisfies the ASC. These two mechanisms are planar. These mechanisms will generate coupling when they are paralleled with the tilting mechanism. A spatial steering mechanism is required to be in parallel with the tilting mechanism due to the nature of the coupling.

H. Shen and D. Zeng et al. have provided theoretical methods for parallel mechanism decoupling [17–19]. N. Amati and Y. Wang have proposed design methods for tilting and steering mechanisms without considering the wheel alignment parameters [8,11]. The method can decouple the vehicle's tilting and steering motion. The steering angles of the wheels on both sides are equal, which cannot satisfy the ASC.

The purpose of this present study is to (a) decouple the parallel tilting and steering mechanism of the vehicle and (b) make the wheels on both sides of the vehicle satisfy the ASC, simultaneously. The main works of this study are as follows:

- A parallel mechanism is proposed. It consists of a spatial steering mechanism and a tilting mechanism in parallel.
- A mathematical model of the parallel mechanism including the wheel alignment parameters has been established. This model is a kinematic model. The decoupling conditions of the parallel mechanism (DCPM) have been solved. A decoupling method is proposed that is based on the model.
- The parameters of the parallel mechanism have been obtained by the use of the mathematical model. These parameters consider both the DCPM and the ASC.
- A prototype has been produced according to the parameters for an experiment. It has been proven by the experiment that the method can reduce the influence of the vehicle's tilting on the steering angle of the wheels. The prototype is able to ensure that the steering angles of the wheels on both sides satisfy the ASC effectively.

2. Mechanism, Model, and Decoupling Method

By establishing a mathematical model for the parallel mechanism, the DCPM has been obtained. This model is a kinematic model.

2.1. The Parallel Mechanism

A spatial steering mechanism that is parallel to the tilting mechanism forms the tilting and steering parallel mechanism. The parallel mechanism is arranged symmetrically about the longitudinal symmetry plane of the vehicle (LSPV). The lengths of all of the symmetrically arranged components are correspondingly equal. The kingpins are set on both sides relative to the frame. As such, the points AB, BO_3, O_3O_4, O_4A, $A'B'$, $B'O_3'$, $O_3'O_4'$, and $O_4'A'$ (per Figure 1) are located on the same plane, which is called the tilt plane of the vehicle (TPV). The plane that is orthogonal to the TPV and containing O_5C is the LSPV. The plane P_H is orthogonal to both the TPV and LSPV. The plane P_H contains O_5. The parallel mechanism is shown in Figure 1. The red part is the spatial steering mechanism; the green part is the tilting mechanism; the blue part is the wheels; and the black part is the frame ($AA'O_4'O_4$) and the other auxiliary lines.
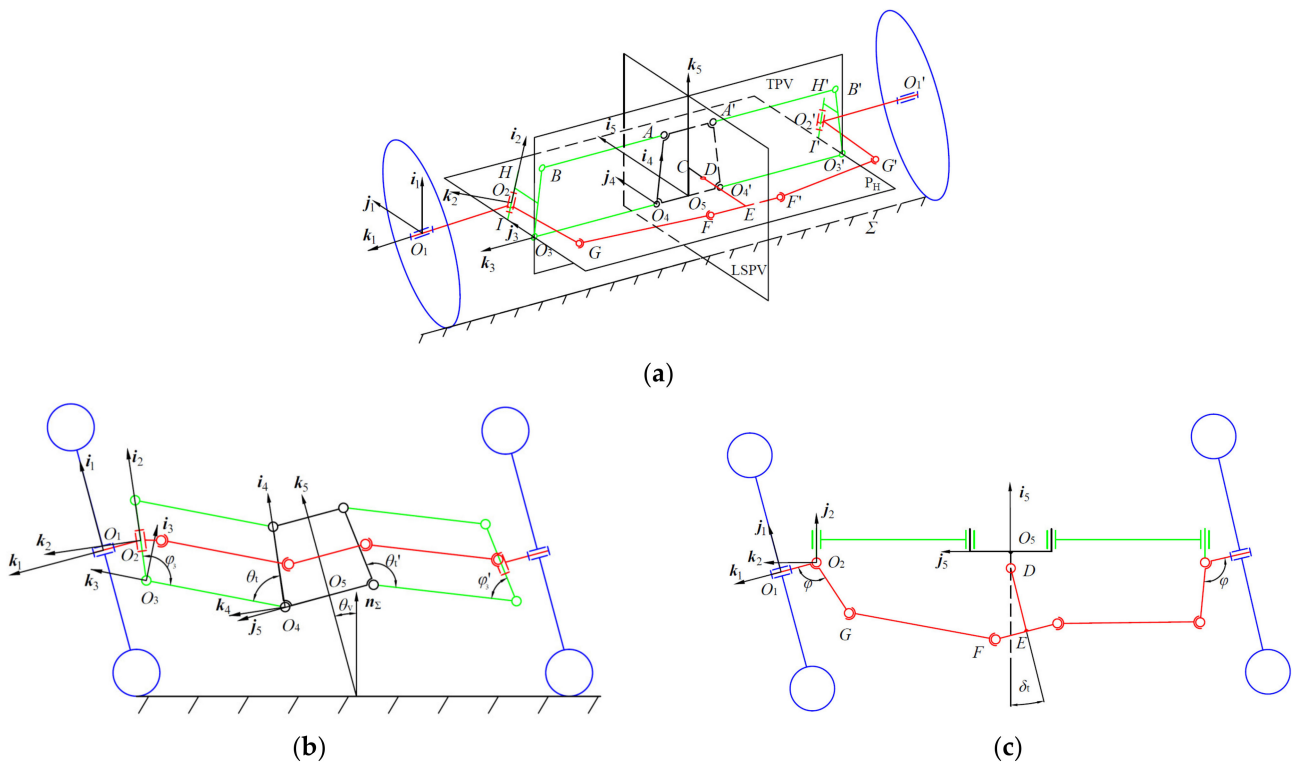

Figure 1. Schematic diagram of the parallel mechanism. (**a**) The parallel mechanism without tilting and turning; (**b**) Projection of the parallel mechanism on the TPV when the vehicle tilts to the left and turns to the left; (**c**) Projection of the spatial steering mechanism on the P_H when the vehicle tilts to the left and turns to the left.

When the tilting mechanism drives the vehicle tilting to the left, the wheel on the left side moves up and the wheel on the right side moves down relative to the vehicle's coordinates. The opposite movement drives the vehicle to tilt to the right.

In the tilting mechanism, the projections of the two kingpins HI and $H'I'$ on the TPV are BO_3 and $B'O_3'$, respectively. HI is fixed to BO_3 and $H'I'$ is fixed to $B'O_3'$. In order to make HI and $H'I'$ translate relative to the frame $AA'O_4'O_4$, the hinges AB, BO_3, O_3O_4 and O_4A form a parallelogram and the hinges $A'B'$, $B'O_3'$, $O_3'O_4'$ and $O_4'A'$ form another parallelogram. These two parallelograms are arranged symmetrically around the LSPV. As such, the lengths of AB, O_3O_4, $A'B'$ and $O_3'O_4'$ are equal and the lengths of BO_3, O_4A, $B'O_3'$ and $O_4'A'$ are equal. The angle between BO_3 (the projections of the lift kingpins HI on the TPV) and O_5C is the inclination angle (φ_i) of the kingpin HI. The angle between the projection of HI on the LSPV and O_5C is the caster angle (φ_b) of the kingpin HI. When the vehicle does not tilt, the angle between O_1O_2 and P_H is the camber angle (φ_c) of the left wheel. When the vehicle does not turn, the angle between the projection of O_1O_2 on

P_H and O_4O_5 is the toe angle (φ_t) of the left wheel. Similarly, the inclination angle and the caster angle of the right kingpin $H'I'$ can be realized and the camber angle and the toe angle of the right wheel can be realized.

In the spatial steering mechanism, points O_1O_2 and O_2G on the steering knuckle are fixed at O_2. O_1O_2 and O_2G rotate around HI. The angle between O_1O_2 and O_2G is φ. Similarly, $O_1'O_2'$ and $O_2'G'$ are fixed at O_2'. $O_1'O_2'$ and $O_2'G'$ rotate around $H'I'$. The angle between $O_1'O_2'$ and $O_2'G'$ is φ, too. FF' turns the wheels on both sides through GF and $G'F'$. G, F, G', and F' are spherical joints. FF' rotates relative to the frame through the hinge of DE and DC. FF' is fixed to DE. DC is fixed to the frame point $AA'O_4'O_4$.

When the parallel mechanism is in motion, the wheels on both sides are steered through δ_t and the vehicle's tilting is realized through θ_t and θ_t'. When the vehicle is not tilting, $\theta_t' = \theta_t = \pi/2 + \varphi_c + \varphi_i$.

2.2. Mathematical Model

The wheels on both sides need to be kept tangent to the ground while tilting. As such, the proposed model uses M/C circular section tires [20], as shown in Figure 2, wherein O_w is the center of the tire section. The radius of the tire section is r_0. The tire radius of O_w is r_w. Taking the left wheel as an example, the mathematical model of the tire tread is established by the application of the circular vector function [21]. When modeling, the tire tread is assumed to be an infinite rigid.
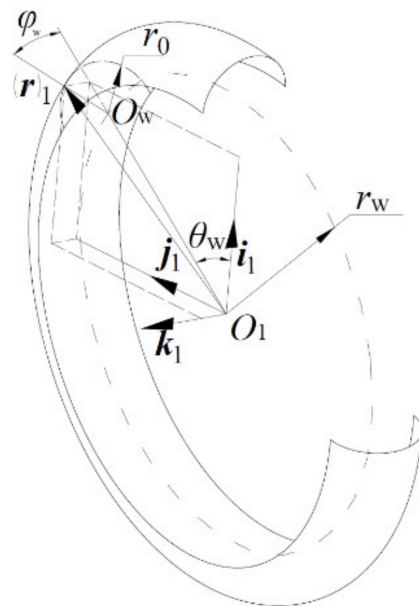

Figure 2. Diagram of the tire tread.

As shown in Figure 2, a right-handed rectangular coordinate $S_1(O_1; i_1, j_1,$ and $k_1)$ is established on the left wheel. The intersection O_1 of the wheel axis and the wheel symmetry plane is the origin of S_1. The point k_1 is along the O_2O_1 direction. The point j_1 is located in the intersection of the horizontal plane and the wheel symmetry plane; j_1 is the same as the forward direction of the wheel. In the S_1, the vector radius r, the unit normal vector n of any point on the tire tread, and the unit vector d in the forward direction of the wheel can be expressed as:

$$\begin{cases} (r)_1 = (r_w + r_0 \cos \varphi_w) e_1(\theta_w) + r_0 \sin \varphi_w k_1 \\ (n)_1 = \left[\frac{\partial (r)_1}{\partial \theta_w} \times \frac{\partial (r)_1}{\partial \varphi_w} \right] / \left| \frac{\partial (r)_1}{\partial \theta_w} \times \frac{\partial (r)_1}{\partial \varphi_w} \right|, \\ (d)_1 = j_1 \end{cases} \tag{1}$$

where $e_1(\theta_w)$ is a circular vector function [21] and θ_w and φ_w are two variables of the tire tread.

A coordinate S_2 (O_2; i_2, j_2, and k_2) is able to be established on the kingpin *HI*, with the steering knuckle O_2 as the origin. The point i_2 is along the O_2H direction and j_2 is parallel to the LSPV and points to the outside of the vehicle. In the S_2, r, n and d can be expressed as:

$$
\begin{cases}
(r)_2 = R(i_2, \delta_2 - \varphi_t)R(j_2, -\varphi_i)R(k_2, \varphi_b)[(r)_1 + |O_2O_1|k_1] \\
(n)_2 = R(i_2, \delta_2 - \varphi_t)R(j_2, -\varphi_i)R(k_2, \varphi_b)(n)_1 \\
(d)_2 = R(i_2, \delta_2 - \varphi_t)R(j_2, -\varphi_i)R(k_2, \varphi_b)(d)_1
\end{cases}, \tag{2}
$$

where δ_2 is an intermediate variable, which represents the angle around *HI* at O_2G. $R(k_2, \varphi_b)$ is the rotation matrix [21].

A coordinate S_3 (O_3; i_3, j_3, and k_3) is then able to be established on O_3O_4, with O_3 as its origin. The point k_3 is along the O_4O_3 direction and j_2 is parallel to the P_H and points to the forward direction of the vehicle. In the S_3, r, n and d can be expressed as:

$$
\begin{cases}
(r)_3 = R\left(j_3, \frac{\pi}{2} - \varphi_3\right)R(k_3, -\varphi_b)[(r)_2 + |IO_2|i_2] + |O_3I|j_3 \\
(n)_3 = R\left(j_3, \frac{\pi}{2} - \varphi_3\right)R(k_3, -\varphi_b)(n)_2 \\
(d)_3 = R\left(j_3, \frac{\pi}{2} - \varphi_3\right)R(k_3, -\varphi_b)(d)_2
\end{cases}, \tag{3}
$$

where φ_3 is an intermediate variable representing the angle between O_3B and O_3O_4.

A coordinate S_4 (O_4; i_4, j_4, and k_4) is established on the frame, with O_4 as its origin. The point i_4 is along the O_4A direction and j_4 is orthogonal to the TPV and points to the forward direction of the vehicle. In the S_4, r, n and d can be expressed as:

$$
\begin{cases}
(r)_4 = R\left(j_4, \frac{\pi}{2} - \theta_t\right)[(r)_3 + |O_4O_3|k_3] \\
(n)_4 = R\left(j_4, \frac{\pi}{2} - \theta_t\right)(n)_3 \\
(d)_4 = R\left(j_4, \frac{\pi}{2} - \theta_t\right)(d)_3
\end{cases}, \tag{4}
$$

The vehicle coordinate S_5 (O_5; i_5, j_5, and k_5) is then established on the frame. O_5 is taken as the origin. The point k_5 is along the O_5C direction, j_5 is along the O_5O_4 direction, i_5 is the intersection of P_H and LSPV, and the direction of i_5 is consistent with that of j_4. In the S_5, r, n and d can be expressed as:

$$
\begin{cases}
(r)_5 = R\left(k_5, -\frac{\pi}{2}\right)R\left(i_5, \varphi_i - \frac{\pi}{2}\right)(r)_4 + |O_5O_4|j_5 \\
(n)_5 = R\left(k_5, -\frac{\pi}{2}\right)R\left(i_5, \varphi_i - \frac{\pi}{2}\right)(n)_4 \\
(d)_5 = R\left(k_5, -\frac{\pi}{2}\right)R\left(i_5, \varphi_i - \frac{\pi}{2}\right)(d)_4
\end{cases}, \tag{5}
$$

The solution method of the intermediate variable δ_2 in (2) is as follows:
In the S_1, O_1G can be expressed as:

$$
(O_1G)_1 = \begin{aligned}&-[|O_1O_2| + |O_2G|\cos(\pi - \varphi)]k_1 \\ &-|O_2G|\sin(\pi - \varphi)j_1\end{aligned}, \tag{6}
$$

Therefore, in the S_5, O_5G can be expressed as:

$$
\begin{cases}
(O_2G)_2 = R(i_2, \delta_2 - \varphi_t)R(j_2, -\varphi_i)R(k_2, \varphi_b) \\
\qquad \times[(O_1G)_1 + |O_2O_1|k_1] \\
(O_3G)_3 = R\left(j_3, \frac{\pi}{2} - \varphi_3\right)R(k_3, -\varphi_b) \\
\qquad \times[(O_2G)_2 + |IO_2|i_2] + |O_3I|j_3 \\
(O_4G)_4 = R\left(j_4, \frac{\pi}{2} - \theta_t\right)[(O_3G)_3 + |O_4O_3|k_3] \\
(O_5G)_5 = R\left(k_5, -\frac{\pi}{2}\right)R\left(i_5, \varphi_i - \frac{\pi}{2}\right)(O_4G)_4 + |O_5O_4|j_5
\end{cases}, \tag{7}
$$

In the S_5, O_5F can be expressed as:

$$(O_5F)_5 = |O_5C|k_5 - |CD|i_5 - |DE|e_5(\delta_t) + |EF|g_5(\delta_t), \tag{8}$$

where $e_5(\delta_t)$ and $g_5(\delta_t)$ are circular vector functions [21].

So, for GF:

$$|GF| = |(O_5F)_5 - (O_5G)_5|, \tag{9}$$

From (9), δ_2 can be expressed as a function of δ_t.

The intermediate variable φ_3 in (3) can be expressed as:

$$\varphi_3 = \pi - \theta_t, \tag{10}$$

The vehicle is arranged symmetrically from left to right. Similarly, the vector radius $(r')_5$, the unit normal vector $(n')_5$ of any point on the tire tread of the right wheel, and the unit vector $(d')_5$ in the forward direction of the right wheel can also be obtained in the S_5.

2.3. The DCPM and the ASC

The conditions that are required for ensuring that HI and $H'I'$ are translated relative to the frame $AA'O_4O_4'$ are:

$$\begin{cases} |AB| = |O_3O_4| = |A'B'| = |O'_3O'_3| \\ |BO_3| = |O_4A| = |B'O'_3| = |O'_3A'| \end{cases}, \tag{11}$$

In order to facilitate the study of the vehicle's tilt motion, it is assumed that the vehicle's pitch angle is zero. As such, the ground plane Σ is parallel to i_5. Then in the S_5, the unit normal vector n_Σ of the Σ can be expressed as:

$$n_\Sigma = \cos\theta_v k_5 - \sin\theta_v j_5, \tag{12}$$

where θ_v is the tilting angle of the vehicle (the angle between k_5 and the Σ).

The vector radius of the two tangent points between the tire treads and Σ satisfy:

$$\begin{cases} [(r)_5 - (r')_5] \cdot n_\Sigma = 0 \\ n_\Sigma = (n)_5 \\ n_\Sigma = (n')_5 \end{cases}, \tag{13}$$

By applying (12) and (13), θ_v and n_Σ can be expressed as a function of θ_t, θ_t', and δ_t.

By applying (1)–(5), given θ_t, θ_t', and δ_t, the left wheel steering angle δ and the right wheel steering angle δ' can be obtained.

$$\begin{cases} \cos\delta = (d)_5 \cdot i_5 \\ \cos\delta' = (d')_5 \cdot i_5 \end{cases}, \tag{14}$$

In order to make δ and δ' independent of θ_v, by the application of (1)–(5), the conditions for eliminating θ_t and θ_t' in (14) are:

$$\begin{cases} [(O_5F)_5 - (O_5G)_5] \cdot (k_3)_5 = |AB| \\ diag(0, \quad 1, \quad 1)[(O_5F)_5 - (O_5G)_5] \times (k_3)_5 = 0 \end{cases}, \tag{15}$$

where

$$(k_3)_5 = R\left(k_5, -\frac{\pi}{2}\right)R\left(i_5, \varphi_i - \frac{\pi}{2}\right)R\left(j_4, \frac{\pi}{2} - \theta_t\right)k_3.$$

In conclusion, (11) and (15) are the DCPM.

For the parallel mechanism that is symmetrically arranged on the left and right sides, the DCPM is described as: (a) when the vehicle is tilting, the two kingpins HI and $H'I'$

translate relative to the frame and (b) when the projections of GF and $G'F'$ in the TPV are parallel and equal as AB and $A'B'$, respectively.

In order to make δ' and δ satisfy the ASC [16] when the vehicle steers left:

$$\frac{L_y}{\tan \delta'} - \frac{L_y}{\tan \delta} = L_x, \tag{16}$$

where L_y is the track width and L_x is the wheelbase.

The steering geometry correction rate (SGCR) of the prototype can be expressed as: [22]:

$$K = \frac{\delta - \delta'}{\delta_0 - \delta'}. \tag{17}$$

where δ_0 is the steering angle of the left wheel and δ_0 is satisfying the ASC.

3. Simulation and Experiment

The parallel mechanism has been analyzed with the use of an example [7]. The parameters of the example are shown in Table 1. The parameters of the rods in the table correspond to the length of the rods. The parameters of the tilting mechanism were directly selected from the literature [7] and the parameters of the frame were designed according to the wheelbase and the track width of the vehicle. The wheelbase of the vehicle is 1.7 m. The track width of the vehicle is 0.89 m.

Table 1. The parameters of the parallel mechanism.

AO_4, $A'O_4'$, BO_3, and $B'O_3'$	AA' and O_4O_4'	AB, $A'B'$, O_3O_4, and $O_3'O_4'$	O_1O_2 and $O_1'O_2'$
175.0 mm	150.0 mm	290.0 mm	80.0 mm
O_2I, $O_2'I'$	O_5C	O_2G, $O_2'G'$	O_3I, $O_3'I'$
88.8 mm	87.5 mm	10.7 mm	81.0 mm
r_0	r_w		
50.0 mm	200.0 mm		
φ_i	φ_b	φ_c	φ_t
7.5 deg	5.5°	1.0°	0.3°

Taking (11), (15), and (16) as the targets to solve, the lengths of DE, FF', $GF(G'F')$, and DC were obtained as 166.1126 mm, 118.7433 mm, 301.4961 mm, and -56.1012 mm (the length of DC is a negative value, which means that point D is in front of the TPV i_5 direction), respectively. The angle of φ was obtained as 99.6721 deg. After all of the parameters of the mechanism were determined, the mathematical model of the tire tread was simulated as is shown in Figure 3.
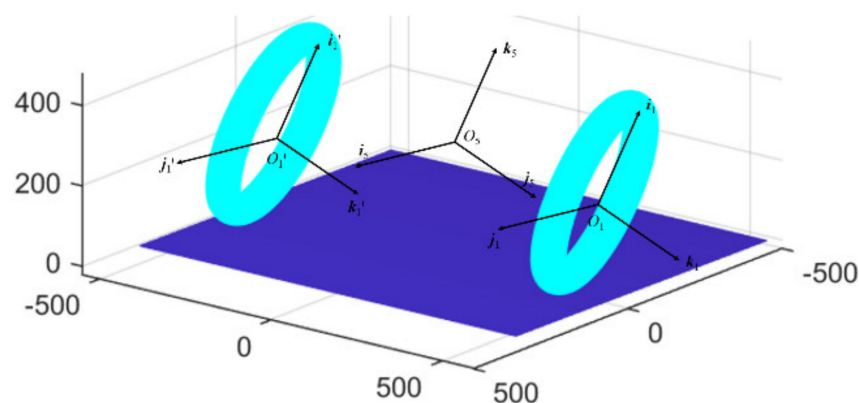

Figure 3. Mathematical model of wheel tire tread.

3.1. Simulation

Through the simulation of the established model, it can be seen that when the vehicle does not tilt, the steering angle of the wheels on both sides is such that is shown in Figure 4.
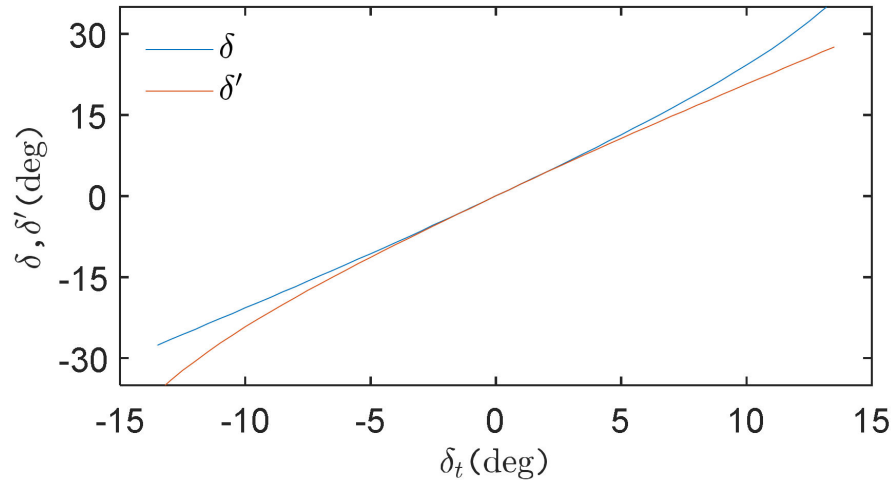

Figure 4. Simulation without tilting.

Taking the process of left steering as an example, compared with when the vehicle is not tilting, the influence of the tilting angle on the steering angles is that which is shown in Figure 5. $\Delta\delta$ and $\Delta\delta'$ represent the errors due to the tilting angle.
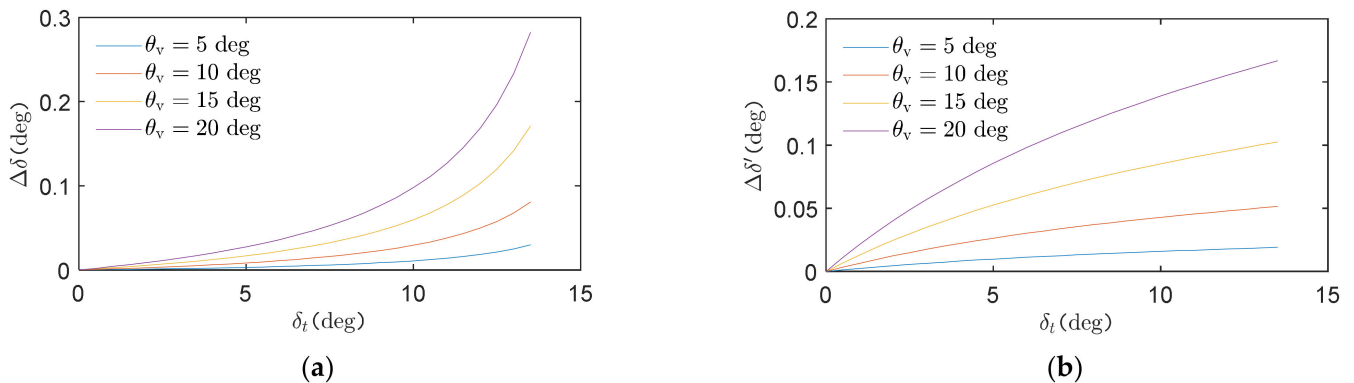
Figure 5. Simulation with tilting. (**a**) The influence of θ_v on δ; (**b**) The influence of θ_v on δ'.

When $|\theta_v| \leq 20$ deg, the maximum error of the outer and inner wheel steering angles is 0.166 deg and 0.282 deg, respectively.

When the vehicle is driving at the speed of $v = 25$ km/h, the target tilting angle is given by [10]. The tilting angle and the steering angles of the wheels on both sides are shown in Figure 6.
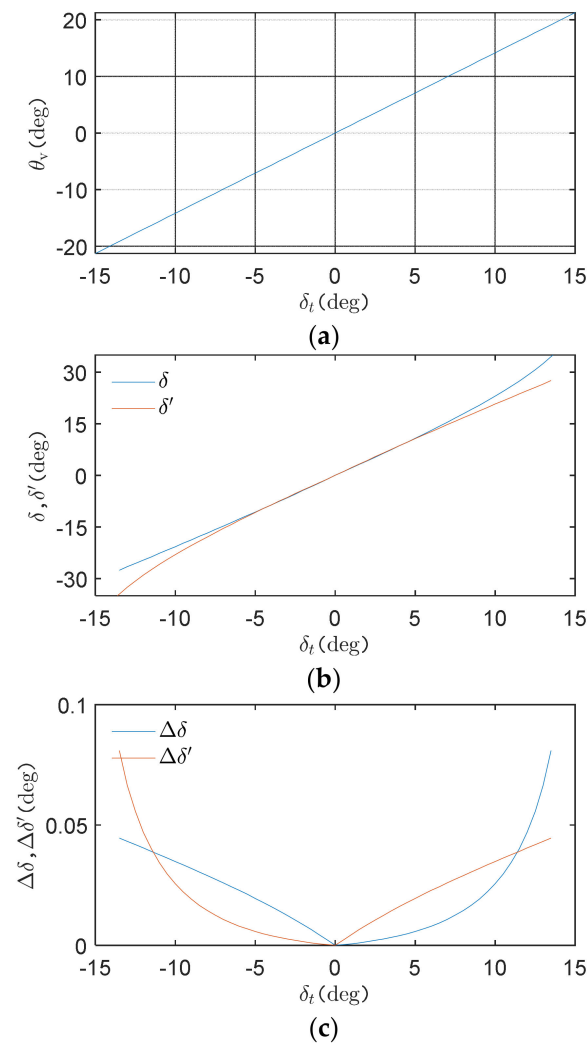
Figure 6. Simulation when the vehicle is driving. (**a**) θ_v when the vehicle is steering; (**b**) δ' and δ when the vehicle is tilting; (**c**) the error in δ' and δ because of the tilting angle.

Since the motion of the vehicle is symmetrical when turning to both sides, the vehicle steering to the left can be taken as an example. The SGCR (*K*) of the vehicle in this context is shown in Figure 7.
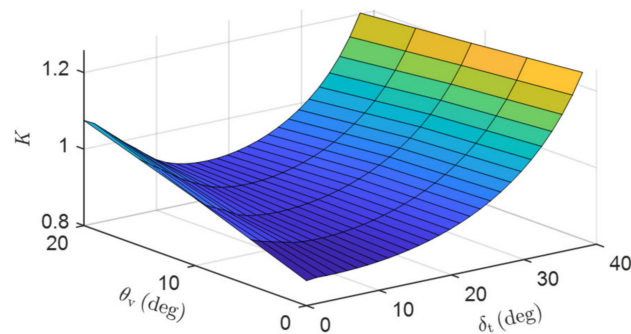

Figure 7. Simulation of the SGCR.

When 0 deg $< \theta_v \leq$ 20 deg and 0 deg $< \delta \leq$ 40 deg, the SGCR of the vehicle is $0.87 \leq K \leq 1.25$. This is within an acceptable range (in low-speed vehicles, *K* should be in the range of $0.4 \leq K \leq 1.6$) [22].

3.2. Experiment

A prototype was produced for the experiment. The proposed parallel mechanism was applied to the prototype. The prototype is shown in Figure 8a. The parallel mechanism is shown in Figure 8b. The parameters of the prototype are the same as those that are shown in Table 1. In order to facilitate the manufacture of the prototype, the parameters that were optimized by the mathematical model were approximated. As such, $DE = 166$ mm, $FF' = 118.7$ mm, $DC = 55$ mm, $GF = G'F' = 301.5$ mm, and $\varphi = 100$ deg. The prototype uses two DC servo motors to drive θ_t and δ_t, respectively. θ_t and δ_t were controlled by a given program. θ_t and θ_t' were linked through the mechanical structure, as are shown by the red part in Figure 8b.
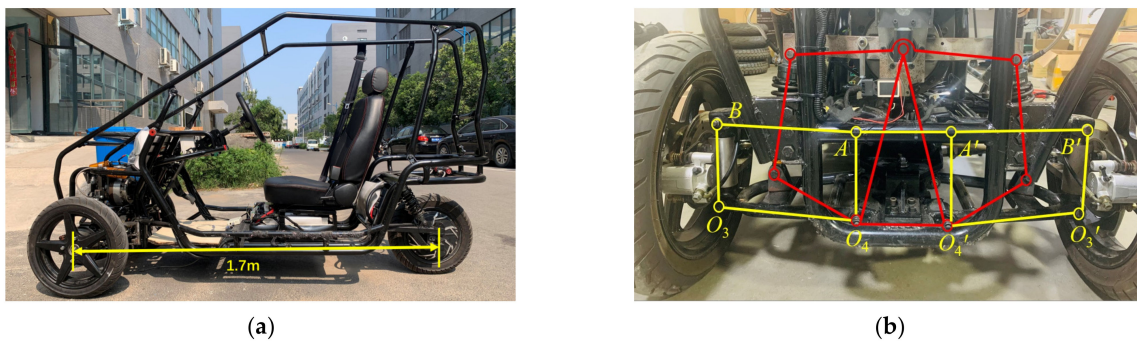

| (a) | (b) |

Figure 8. The prototype. (**a**) The prototype; (**b**) The parallel mechanism.

The manner that was used to read and record the experiment data is shown in Table 2. The equipment of the experiment is shown in Figure 9.

Table 2. Equipment list of the experiment.

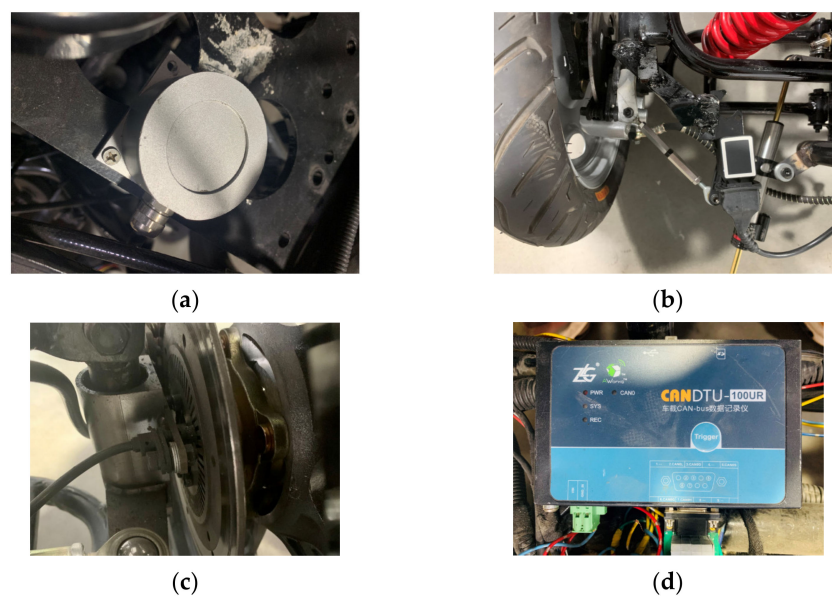| Function	Hardware
Read θ_v, yaw rate $\dot{\varphi}_v$, and fit trajectory. Read δ_t, δ, and δ'. Read v. Record the experimental data.	Inertial measurement unit: VG427C-CAN. Angle sensor: KD-701. Wheel speed sensor: TE-ABS-181. Data logger: CANDTU-100UR.

| (a) | (b) |
| (c) | (d) |

Figure 9. The equipment of the experiment. (**a**) Inertial measurement unit; (**b**) angle sensor; (**c**) wheel speed sensor; (**d**) data logger.

Taking the prototype steering left as an example, the prototype drives on the road with the same δ_t and v, but different θ_v, where the speed is $v = 25$ km/h. The results of the experiment are shown in Figure 10.
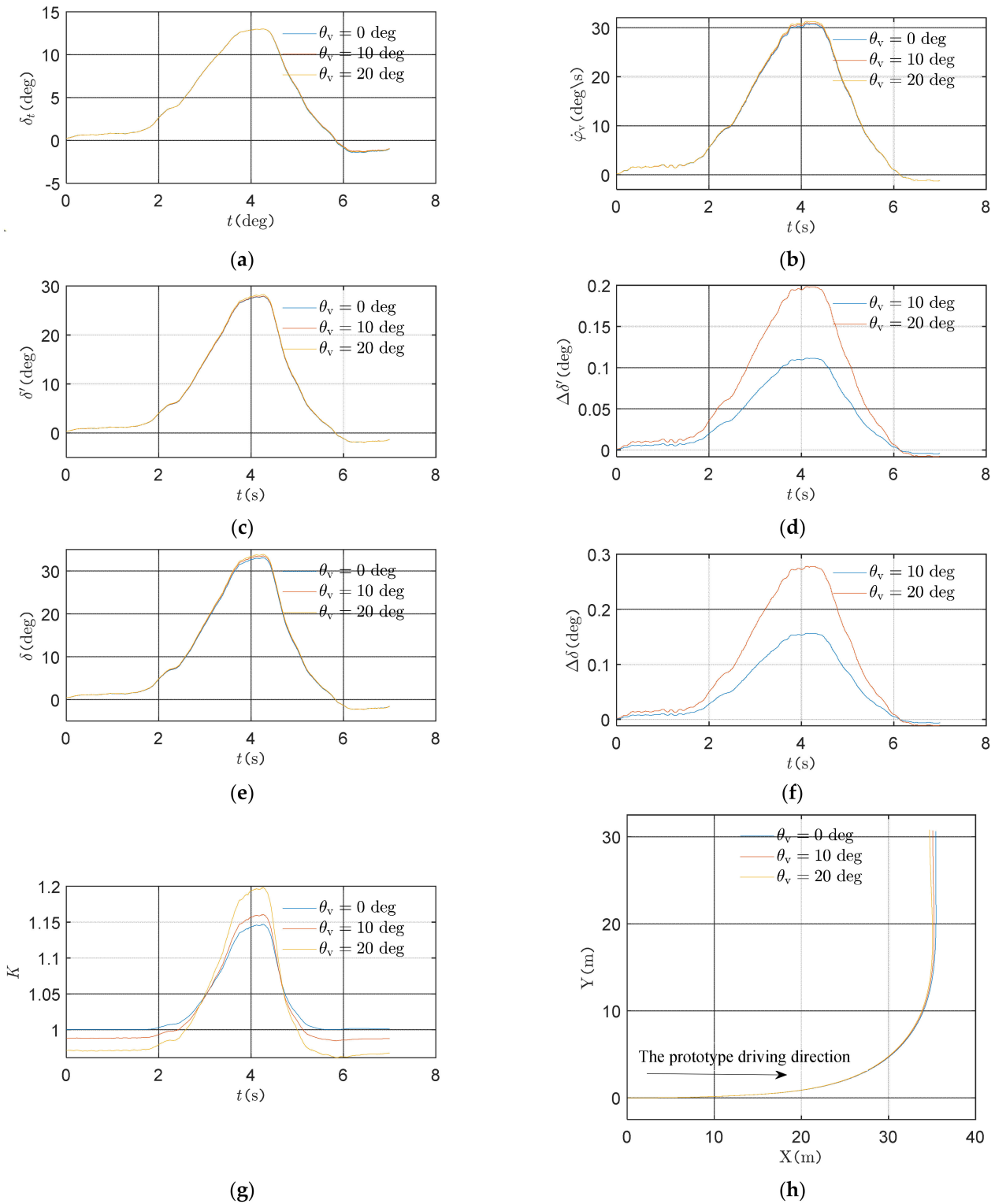

Figure 10. The result of the experiment. (**a**) Entered steering information; (**b**) the yaw rate of the prototype; (**c**) steering angle of the left wheel; (**d**) steering angle of the right wheel; (**e**) steering angle error of the left wheel; (**f**) steering angle error of the right wheel; (**g**) the SGCR; (**h**) the trajectory.

The δ_t and θ_v values that were obtained by the experiment were input into the mathematical model. The δ and δ' values that were calculated by the model were compared with the results of the experiment. The average relative errors of the steering angles are shown in Table 3.

Table 3. Comparison of theory and the experiment.

	θ_v = 0 deg	θ_v = 10 deg	θ_v = 20 deg
δ'	0.46%	0.69%	0.91%
δ	0.51%	0.77%	1.07%

In order to facilitate the manufacture of the prototype, the mechanism's parameters were approximated. The established mathematical model is infinitely rigid, ignoring the effects of vehicle dynamics. The experiment made the prototype drive at a constant speed with different tilting angles in order to dilute the influence of the nonlinear change of the tires. These three points are the main reasons for the errors in the experiment.

Compared with θ_v = 0 deg, the maximum relative errors of the steering angles, the yaw rate, and the trajectory of when the prototype drove at different tilting angles are shown in Table 4.

Table 4. The influence of prototype tilting on steering.

	δ'	δ	$\dot{\varphi}_v$	Trajectory
θ_v = 10 deg	0.45%	0.57%	0.98%	1.04%
θ_v = 20 deg	0.64%	0.78%	2.49%	2.09%

The parallel mechanism that was designed by this method can reduce the influence of the vehicle tilting on the steering angle of the outer and inner wheels by up to 0.64% and 0.78%, respectively. This shows that when the vehicle is traveling at a low, constant speed, the influence of the vehicle tilting on the steering angle is small. In contrast, vehicle tilting affects the inner wheels more so than the outer wheels. As the vehicle's tilting angle increased, the influence of the vehicle tilting on the steering angle was greater. This effect is most obvious in the yaw rate. When θ_v = 20 deg, the relative error of the yaw rate was 2.49%. This effect eventually appeared on the trajectory; with θ_v = 20 deg, the relative error of the trajectory was 2.09%.

The SGCR of the prototype is shown in Table 5.

Table 5. The SGCR.

	θ_v = 0 deg	θ_v = 10 deg	θ_v = 20 deg
Maximum	1.146	1.160	1.198
Average	1.031	1.025	1.016

The SGCR of the prototype is between 1.198 and 0.961. For low-speed vehicles, this is an acceptable range [22]. The characteristics of the vehicle when it is in operation at high speed have yet to be verified. When K = 1, the ASC is completely satisfied. When the tilting angle increases, the deviation of the value of K from 1 also became larger, but it was always within an acceptable range.

4. Discussion

The presently established mathematical model is infinitely rigid, ignoring the effects of vehicle dynamics. The low-speed experiments verified the kinematics of the proposed parallel mechanism. The experiment had the prototype drive at a low, constant speed with different tilting angles in order to dilute the influence that is caused by the nonlinear change of the tires. The dynamic properties of the proposed parallel mechanism and the dynamic interaction between the parallel mechanism and the vehicle require further research.

The experiment has verified that the proposed model is correct. The parallel mechanism that was designed by this method can reduce the influence of vehicle tilting on the steering angle of the outer and inner wheels by up to 0.64% and 0.78%, respectively. The SGCR of the prototype is between 1.198 and 0.961. This is an acceptable range [22]. The experimental results satisfied the purpose of this study.

The parallel mechanism that was designed by the application of this method can change the steering geometry by adjusting the φ value and the lengths of *DE* and *DC*, such that δ and δ' satisfy the ASC corresponding to different wheelbases.

The proposed method decouples the spatial parallel mechanism effectively. It also provides an ATV suspension design method. The present study's method is suitable for decoupling various spatial parallel mechanisms.

The mathematical model includes wheel alignment parameters but it does not include the shock absorber. The shock absorber also influences the movement of the parallel mechanism. Future research should include the deformation of the shock absorber.

5. Conclusions

1. This paper proposes a tilting and steering parallel mechanism. The proposed parallel mechanism consists of a spatial steering mechanism and a tilting mechanism. The parallel mechanism can be used as the suspension for ATV.
2. This study establishes a mathematical model that may be used to analyze the DCPM. The model is infinitely rigid, ignoring the effects of vehicle dynamics. This model is a kinematic model. A decoupling method has been proposed that is based on the model.
3. The effectiveness of the decoupling method has been proven by an experiment on a prototype. The low-speed (25 km/h) experiments verified the kinematics of the proposed parallel mechanism. The prototype can reduce the influence of vehicle tilting on the steering angle of the outer and inner wheels by up to 0.64% and 0.78%, respectively. The SGCR of the prototype is between 1.198 and 0.961.
4. The proposed parallel mechanism that is based on the proposed decoupling method simultaneously achieves the following purposes: a) ignoring the effects of the nonlinear change of the tires, (b) decoupling the tilting and steering parallel mechanism of the vehicle, and (c) making the wheels on both sides of the vehicle satisfy the ASC.

6. Patents

There are patents resulting from the work that is reported in this manuscript. The numbers of these patents are CN110509994B, CN109353405B, CN113479261A, CN113443007A, and CN112172921A.

References

1. Navikas, D.; Pitrėnas, A. Determination and Evaluation of a Three-Wheeled Tilting Vehicle Prototype's Dynamic Characteristics. *Appl. Sci.* **2022**, *12*, 5121. [CrossRef]
2. Haraguchi, T.; Kageyama, I.; Kaneko, T. Study of Personal Mobility Vehicle (PMV) with Active Inward Tilting Mechanism on Obstacle Avoidance and Energy Efficiency. *Appl. Sci.* **2019**, *9*, 4737. [CrossRef]
3. Haraguchi, T.; Kageyama, I.; Kaneko, T. Inner Wheel Lifting Characteristics of Tilting Type Personal Mobility Vehicle by Sudden Steering Input. *Jido Sha Gijutsukai Ronbunshu* **2019**, *50*, 96–101. [CrossRef]
4. Kashem, S.; Saravana, K. Comprehensive study on suspension system and tilting vehicle. *Aust. J. Basic Appl. Sci.* **2015**, *9*, 46–53.
5. Li, H.; Gao, R.; Li, X.; Zhang, J.; Wang, Y.; Wei, W. Vehicle Tilting Control Method. Patent No. CN 111231935 A, 13 January 2020.
6. Karamuk, M.; Alankus, O.B. Development and Experimental Implementation of Active Tilt Control System Using a Servo Motor Actuator for Narrow Tilting Electric Vehicle. *Energies* **2022**, *15*, 1996. [CrossRef]
7. Liu, P.; Li, X.; Gao, R.; Li, H.; Wei, W.; Wang, Y. Design and experiment of tilt-driving mechanism for the vehicle. *J. Jilin Univ.* **2022**. [CrossRef]
8. Haraguchi, T.; Kaneko, T.; Kageyama, I. A Study of Steer Characteristics of Personal Mobility Vehicle (PMV) with Inward Tilting Mechanism. *Trans. Soc. Automot. Eng. Jpn.* **2022**, *53*, 58–64.
9. Matsuda, M.; Kageyama, I.; Kuritagawa, Y.; Haraguchi, T.; Kaneko, T.; Kobayashi, M.; Murayama, T. Study on Driving Behavior Considered Vehicle Characteristics of Personal Mobility Vehicle with Lean Mechanism. In Proceedings of the Japan Society of Mechanical Engineers, Transportation and Logistics Conference, Tokyo, Japan, 21 January 2019; pp. 96–101.
10. Liu, P.; Ke, C.; Gao, R.; Li, H.; Wei, W.; Wang, Y. Design and Test of Active Roll Vehicle. *Automot. Eng.* **2020**, *42*, 1552–1557 + 1584. [CrossRef]
11. Wang, Y.; Wei, W.; Li, H. Vehicle Steering Tilt Combined Mechanism and Active Tilting Vehicle Using the Mechanism. Patent No. CN110386216A, 29 October 2019.
12. Shino, K. Active Tilting Vehicle. Patent No. CN110386216A, 22 September 2020.
13. Cho, Y.H.; Kim, J.-H. Design of Optimal Four-Wheel Steering System. *Veh. Syst. Dyn.* **1995**, *24*, 661–682. [CrossRef]
14. Sun, Q.H.; Dong, E.G.; Zhang, L.; Gao, S.R. Parameters analysis and optimal design of four-bar steering mechanism. *J. Liaoning Tech. Univ.* **2007**, *26*, 278–280.
15. Bian, X.L.; Song, B.A.; Becker, W. The optimization design of the McPherson strut and steering mechanism for automobiles. *Forsch. Im Ing.* **2003**, *68*, 60–65. [CrossRef]
16. Zhao, J.-S.; Liu, X.; Feng, Z.-J.; Dai, J.S. Design of an Ackermann-type steering mechanism. *Proc. Inst. Mech. Eng. Part C J. Mech. Eng. Sci.* **2013**, *227*, 2549–2562. [CrossRef]
17. Shen, H.; Wu, C.; Chablat, D.; Wu, G.; Yang, T.-L. Topological design of an asymmetric 3-translational parallel mechanism with zero coupling degree and motion decoupling. In Proceedings of the ASME 2018 International Design Engineering Technical Conferences & Computers and Information in Engineering Conference, Quebec City, QC, Canada, 26–29 August 2018; pp. 7–38.
18. Shen, H.; Chablat, D.; Zeng, B.; Li, J.; Wu, G.; Yang, T.-L. A Translational Three-Degrees-of-Freedom Parallel Mechanism with Partial Motion Decoupling and Analytic Direct Kinematics. *J. Mech. Robot.* **2020**, *12*, 021112–021119. [CrossRef]
19. Zeng, D.; Wang, H.; Fan, M.; Wang, J.; Hou, Y. Type Synthesis of Three Degrees of Freedom Rotational Generalized Decoupling Parallel Mechanism. *J. Mech. Eng.* **2017**, *53*, 17–24. [CrossRef]
20. General Administration of Quality Supervision, Inspection and Quarantine of the People's Republic of China. *GB/T 2983-2015 Series of Motorcycle Tyres*; General Administration of Quality Supervision, Inspection and Quarantine of the People's Republic of China: Beijing, China, 2015.
21. Dong, X.; Li, H.; Wei, W. *Theory and Application of Gear Meshing with Double Degrees of Freedom*; China Machine Press: Beijing, China, 2011.
22. Wang, X. *Automotive Chassis Design*; Tsinghua University Press: Beijing, China, 2014.